


Effects of number of inlet guide vanes on the aerodynamic performance of a centrifugal compressor

Proc IMechE Part A:
J Power and Energy
0(0) 1–14
© IMechE 2021
Article reuse guidelines:
sagepub.com/journals-permissions
DOI: 10.1177/09576509211026824
journals.sagepub.com/home/pia



M Anbarsooz¹ , M Amiri², A Erfanian² and E Benini³

Abstract

Variable inlet guide vanes (VIGVs) are widely used for flow throttling and also extending the operating range of centrifugal compressors. Although there are several studies on the effects of adding IGVs on the performance curve of the compressors, none of them have focused on the number of vanes. In the current study, high-fidelity three-dimensional numerical simulations are carried out to analyze the effects of adding VIGVs with different number of vanes on the aerodynamic performance of a single-stage centrifugal compressor. The selected compressor prototype is a high flowrate single-stage compressor equipped with a vaned diffuser, designed and fabricated by Siemens. Computational fluid dynamic simulations are performed for three different number of guide vanes at three IGV inclination angles of 0, -30 and $+45$ degrees. The numerical results are validated by comparing the pressure-rise curves with the available experimental data of the compressor data sheet, where a good agreement was achieved. Results show that at the fully-open condition, the number of vanes does not have considerable effect on the performance curve of the compressor. However, as the IGV inclination angle increases, the number of inlet vanes plays a considerable role in the compressor efficiency. For example, at IGV inclination angle of $+45$ degree, increasing the number of vanes from 7 to 11 can increase the compressor maximum efficiency up to 5 points. Numerical results showed that increasing the number of inlet guide vanes imposes a higher pressure drop in the inlet passage of the compressor while generating a more uniform velocity distribution at the suction surface of the impeller. Due to the existence of several counteracting effects, an optimum number of inlet guide vanes can be found.

Keywords

IGV, CFD, centrifugal compressor, blade angle, Mach number

Date received: 22 January 2021; accepted: 1 June 2021

Introduction

Centrifugal compressors are among the vital components in a wide range of industries such as the oil refineries, petrochemical plants, natural gas processing plants and power generation. In almost all of these applications, compressors meet variable working conditions. Hence, a compressor's ability to deal with a wider flow range makes it superior to the others. To make a compressor deal with variable working conditions various regulation methods have been used such as the rotation speed variations, upstream suction throttling, flow bypassing, adjusting diffuser vanes and adjusting the *Inlet Guide Vanes* (IGVs).

Traditionally, IGVs were used at the compressor inlet to guide the flow towards the impeller with a desired inlet angle. They have also been used to impose positive/negative prewhirls to regulate the stage pressure rise and flow rate, resulting in

decreasing/increasing the relative Mach number at the inducer tip.¹ Although there are many studies on the fluid dynamics of the compressor impeller^{2–11} and diffuser^{12–18} the studies on the flow details of a centrifugal compressor equipped with an IGV are relatively scarce. What follows is a brief review on the main studies on the effects of IGVs on the performance of centrifugal compressors.

¹Department of Mechanical Engineering, Quchan University of Technology, Quchan, Iran

²Research and Development Department, Parto Sanat Pash (PSP) Company, Mashhad, Iran

³Dipartimento di Ingegneria Industriale, Università di Padova, Padova, Italy

Corresponding author:

M Anbarsooz, Quchan University of Technology, Quchan 9477177870, Islamic Republic of Iran.

Emails: m.anbarsooz@gmail.com; anbarsooz@qiet.ac.ir

Rodgers¹⁹ experimentally studied the effects of adjustable inlet guide vanes on the performance of a single stage, moderately high specific speed and high inducer Mach number centrifugal compressor with a vaned diffuser. Their experimental measurements revealed that the impeller stability and the compressor surge margin were considerably enhanced, even though the vaned diffuser was operating in the stall condition.

Ishino et al.²⁰ developed and tested variable inlet guide vanes for an automobile turbocharger. Their VIGV had 6 vanes and the vanes setting angles could be varied from 0 to 60 degrees. Their experimental data showed that the added prewhirl enhances the efficiency and surge characteristics of the tested turbocharger.

Mohtar et al.^{21,22} experimentally determined the performance curves of a turbocharger compressor equipped with a casing treatment and variable inlet guide vanes at École Centrale de Nantes. The tested impeller had 6 main blades and 6 splitter blades, equipped with a twelve flat-bladed VIGV system. Their measurements showed that their map width enhancement system was able to increase the compressor pressure ratio at high rotational speeds, however, it failed in extending the compressor's operating flow range.

Toussaint and Podevin²³ added variable inlet guide vanes to an automotive turbocharger to increase its rotational velocity and as a result, reduce the turbo-lag of the engine especially at lower engine speeds. Their results showed that this concept can reduce the turbo-lag at engine's partial loads larger than 40%. At lower partial loads, however, no considerable decrease in the engine turbo-lag was observed.

Xiao et al.²⁴ numerically analyzed the effects of adding variable inlet guide vanes (VIGVs) on the performance curves and velocity vectors of a single stage compressor impeller. The tested impeller had 11 main blades and 11 splitters. The IGV system consisted of 8 straight blades with a NACA-m3 cross section profile. Their numerical results showed that the performance curves shift towards smaller flow rates when IGVs turn positive and vice versa. However, no validation for the numerical results was presented.

Zemp et al.²⁵ performed unsteady numerical simulations to analyze the blade force response in a centrifugal compressor due to inlet distortions caused by struts, duct bends or IGVs. Their simulation results indicated that the inlet distortions can increase the maximum value of the forcing function up to 30%, compared to the actual inlet flow distribution.

Tan et al.²⁶ performed three-dimensional numerical simulations to examine the effects of radial inlet on a VIGV performance in a single-stage centrifugal compressor and compared the results with the axial inlet condition. The tested impeller had 19 blades and the IGV consisted of 14 multi-arc airfoil blades. Their numerical data showed that in the case of radial inlet, the overall polytropic efficiency and the total pressure ratio was decreased 4% and 3.3%, respectively. It was

due to the flow non-uniformity induced by the radial inlet and the flow losses in the radial inlet.

As reviewed above, most of the studies have focused on the effects of adding a certain IGV system on the performance curves of centrifugal compressors and there was no investigation on the effects of the number of inlet guide vanes on the pressure rise and efficiency of the compressor. High-fidelity Computational Fluid Dynamics (CFD) simulations²⁷ are performed in the current study to reveal various aspects of the complex flow inside the compressor in the presence of VIGVs. The numerical results are first validated against the experimental data of a high-flow rate single-stage centrifugal compressor, where a convincing agreement was observed. Then, the numerical simulations are carried out for various numbers of the inlet guide vanes and the resultant flow characteristics are analyzed. This paper is organized in four sections. In the next section, the geometrical and operational specifications of the studied compressor are presented. Then, the numerical setup containing the computational domain, grid generation, boundary conditions and solver settings is presented. The results of the numerical simulations and the corresponding discussions are presented in the final section.

Description of the studied centrifugal compressor

The studied compressor is a STC-GO type, single-stage centrifugal compressor designed and fabricated by Siemens (note: <https://www.siemens.com/>). The operating fluid is a gas mixture, mainly consisting of methane. Table 1 reports the composition of the operating gas mixture. The operating conditions of the design point are given in Table 2. The gas mixture inlet pressure is 2.50 bar and the total pressure ratio at the design point is 1.288. Figure 1 shows the meridional contour, blade angle distributions and the axial view of the impeller. The hub, suction and tip diameters of the impeller are 0.142, 0.434 and 0.618 m, respectively. The impeller has 14 blades with an axial length of 0.216 m. The compressor is equipped with a vaneless and a vaned diffuser. The vaneless diffuser starts from the tip of the impeller up to a diameter of 0.71 m, where there are the leading edges of the 20 vanes of the vaned diffuser. The cross-sections of the diffuser vanes are Drela AG10 airfoil (note: https://m-selig.ae.illinois.edu/ads/coord_database.html). The IGV axis is located 0.36 m upstream of the impeller suction. As shown in Figure 2, it consists of 11 blades which are able to rotate from -60° up to $+60^\circ$, owing to a geared rotating mechanism. The cross sections of the IGVs are NACA0010, with a chord length of 0.0139 m at the hub and 0.1673 m at the shroud. The geometrical dimensions of the impeller, diffuser and IGV are presented in Table 3.

Numerical setup

Governing equations and computational domain

The governing equations are the steady Reynolds-averaged Navier-Stokes equations for the turbulent flow of a compressible Newtonian fluid. The continuity, momentum and energy equations are solved in

Table 1. The composition of the operating gas mixture.

Gas component	Volumetric fraction (%)
Methane	67.57
Hydrogen	22.71
Nitrogen	4.36
Water	2.73
Carbon mono-oxide	1.84
Carbon dioxide	0.79

Table 2. Operating conditions.

Parameter	Value	Unit
Inlet pressure	2.50	bar (absolute)
Inlet temperature	45.0	°C
Inlet volumetric flow rate	45,827	m ³ /h
Inlet mass flow rate	60,089	kg/h
Discharge pressure	3.22	bar (absolute)
Discharge temperature	70.0	°C
Rotational speed	9,531	rpm
Shaft power	1,032	kW

conjunction with the transport equations of an appropriate turbulence model for closing the set of equations. The Realizable $k-\varepsilon$ turbulence model is employed in this study which has proven to be suitable for numerical simulation of centrifugal compressors.²⁸ The solution of the governing equations is obtained using the Ansys-Fluent R19.0 software.^{29,30}

The computational domain consists of three zones, (a) the inlet stationary zone containing the IGVs, (b) the impeller rotating zone and (c) the diffuser stationary zone. As shown in Figure 3(a), the inlet zone is divided into 11 mesh zones, the impeller zone into 14 and the diffuser zone is divided into 20 subzones. These zones are connected via mixing planes.³¹ It must be noted that the radial clearance between the IGV tip and the casing is very small (about 0.1 mm) and the stem connecting the turning mechanism to the IGV is located between the IGV tip and the casing. Therefore, the radial clearance between the IGV and the casing is neglected in the numerical simulations.

The central core in the IGV zone is blanked out to create a mapped grid. The radius of the central core is 0.01 m which means the area of the central core is less than 0.02% of the inlet area (inlet diameter is 0.8 m). In the IGV zone, span 0 starts from $r = 0.01$ m.

Boundary conditions

The applied boundary conditions are shown in Figure 3(b). At the beginning of the inlet stationary zone, a uniform total pressure ($P_0 = 250$ kPa) and total

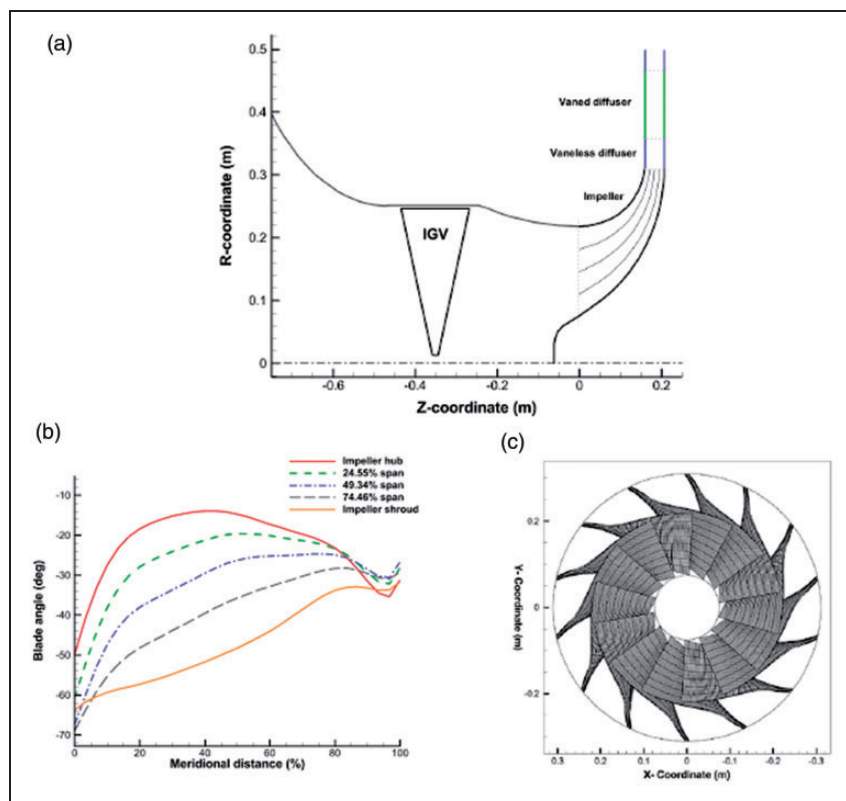


Figure 1. (a) The meridional contour (b) blade angle distributions and (c) the axial view of the studied impeller.

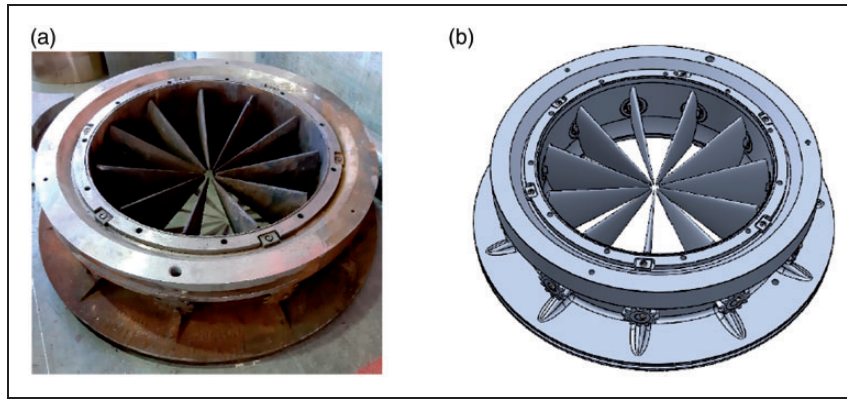


Figure 2. (a) Real and (b) modeled IGV.

Table 3. Geometrical dimensions of the IGV, impeller and diffuser.

Parameter	Value	Unit
Impeller hub diameter	0.142	m
Impeller suction diameter	0.434	m
Impeller tip diameter	0.613	m
Impeller axial length	0.216	m
Impeller number of blades	14	–
Vaneless diffuser diameter	0.710	m
Diffuser diameter	0.99	m
Diffuser number of blades	20	–
IGV inlet diameter	0.50	m
IGV number of blades	11	–

temperature ($T_0=318\text{K}$) are set. The inlet stationary zone and the impeller rotating zone are connected via a mixing plane, where all the transport properties (density, velocity components, temperature, turbulence quantities, etc.) are conserved.³² This method ensures a steady flow in both frames of reference. This approach has been validated and used by many researchers.^{31,33–35} A similar boundary condition is used to connect the impeller rotating zone to the diffuser stationary zone.³⁶ No-slip wall boundary condition is applied on the hub, shroud and impeller blade surfaces. At the outlet surface of the diffuser zone a uniform velocity distribution is imposed according to the desired mass flow rate. The computed total pressure at this surface is reported to calculate the total-total pressure ratio when the solution reaches the steady-state condition.

The flow coefficient, φ , work coefficient, ψ , and specific speed, N_s , for a compressor are defined as:³⁷

$$\varphi = Q/ND^3 \quad (1)$$

$$\psi = gH/N^2D^2 \quad (2)$$

$$N_s = \frac{NQ_s^{1/2}}{H^{3/4}} \quad (3)$$

where Q is the volumetric flow rate, N the rotational speed, D the impeller diameter and H is the adiabatic head. For the current compressor, the corresponding flow coefficient, work coefficient and specific speed are 0.00580, 0.00145 and 56.93, respectively. The compressor torque-based total-total efficiency is also defined as:³⁸

$$\eta = \frac{m \cdot h_{02s} - h_{01}}{T\omega} \quad (4)$$

where $m_{\dot{}}$ is the compressor mass flow rate, h_{02s} is the isentropic total enthalpy at the compressor outlet, T is the calculated shaft torque, ω is the angular velocity and h_{01} is the total enthalpy at the compressor inlet.

Grid generation

The computational domain is discretized using H-type elliptic cells. Three grid resolutions are tested, named as coarse, medium and fine grids. The number of computational cells in the IGV, impeller and diffuser zones for each of the grid resolutions as well as the total number of cells are presented in Table 4. An enhanced wall treatment available in Ansys-Fluent software is employed which is insensitive to the wall y^+ .³⁹ A schematic of the medium grid resolution is shown in Figure 4, where the grid topology close to the impeller's blade tip is magnified. The numerical results corresponding to each grid resolution are given in 'Results and discussions' section.

Solver settings

The pressure and velocity equations are solved simultaneously using the coupled approach available in Ansys-Fluent software.³² Least square cell-based method is used for evaluating the gradients and the discretization of the pressure, density, momentum and turbulence equations are done using the second order upwind scheme.

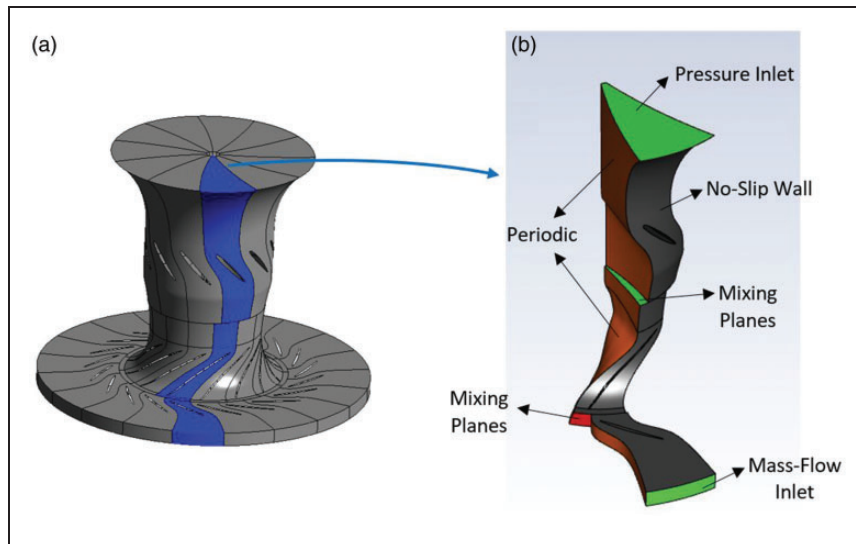


Figure 3. (a) Computational domain and (b) boundary conditions.

Table 4. Details of the three grid resolutions.

Grid Name	Number of nodes in IGV zone	Number of nodes in impeller	Number of nodes in diffuser zone	Total number of Nodes
Coarse	42,160	222,720	66,940	331,922
Medium	77,066	407,040	123,839	607,945
Fine	119,328	629,760	190,779	939,867

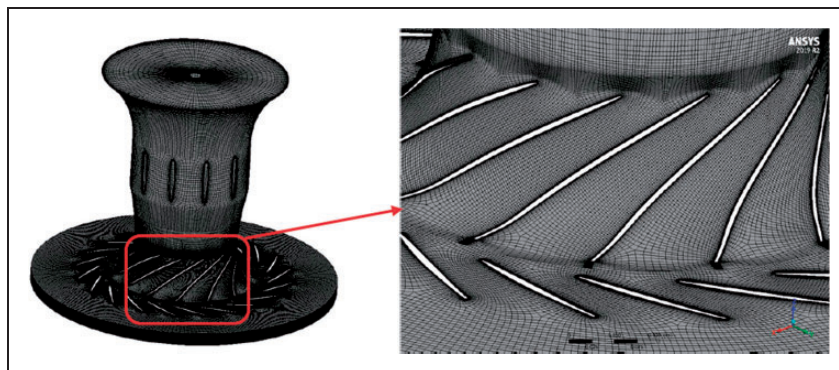


Figure 4. Medium grid resolution.

Results and discussions

The results of the grid sensitivity analysis are presented in Figure 5. In this figure, the pressure distribution on a central line located on the outlet surface of the diffuser zone is plotted for the three tested grid resolutions. As can be seen in the figure, the average difference between the pressure distributions obtained by the medium and fine grids is less than 0.3%. As a result, the medium grid is selected for the rest of the computations. The average y^+ value on the impeller blade of this grid resolution is 37, which is in the acceptable range of standard wall-functions and ensures that the first cell is in the buffer zone.⁴⁰

The numerical results for the pressure ratio as a function of the mass flow rate at various angles of the IGVs are compared with the experimental data in Figure 6. The experimental data is adopted from the compressor data-sheet, where the compressor curves were reported for $\lambda_{IGV} = 0^\circ, -30^\circ$ and $+45^\circ$. The figure shows that there is a convincing agreement between the numerical results and those of the experiments in almost all of the simulated points. The average error between the numerical results and those of the experiments is less than 2%.

The positive angle of the IGVs generates a prewhirl velocity in the rotor's direction of rotation and as a

result, the work done on the fluid by the impeller decreases. Conversely, the negative angle of the IGVs has increased the compressor head by generating a circumferential velocity component in the opposite direction of the impeller rotation. The lower pressure ratio of the positive IGV requires a larger velocity to maintain the desired mass flow rate. As a result, the choke mass flow rate decreases as the IGV angle increases. Conversely, the negative IGV angle improves the choke mass flow rate.

As can be seen in Figure 6, at lower pressure-ratio values across the map (e.g., $\lambda_{IGV} = -45^\circ$) the compressor surge margin has decreased and the compressor can work safely at lower flow rates. It is mainly because at a constant flow rate, the larger pressure-rise means a larger positive pressure gradient in the streamwise direction and this can anticipate compressor stall. Furthermore, positive prewhirl results in lower incidence angles at the impeller leading edge especially at lower flow rates.⁴¹ In other words, positive IGV angle delays separation at near surge operating conditions and enhances the impeller stability at low flow rates.

In Figure 6, the numerical results of the compressor performance curve without the presence of the IGVs and with the presence of the IGVs at the fully-open condition (zero-inclination angle, $\lambda_{IGV} = 0^\circ$) are depicted. Subtracting these two curves from each other is a measure of the pressure-drop caused by adding IGVs at the fully-open condition ($\lambda_{IGV} = 0^\circ$).

Unfortunately, the experimental data on the compressor efficiency are not provided by the manufacturer and as a result, the numerical results for the efficiency cannot get double-checked with the experimental data. However, the employed numerical methodology and its underlying assumptions have been validated for the Eckardt compressor⁴² (both the pressure ratio and the total-total efficiency) in a previous paper and therefore, the results are not repeated here.

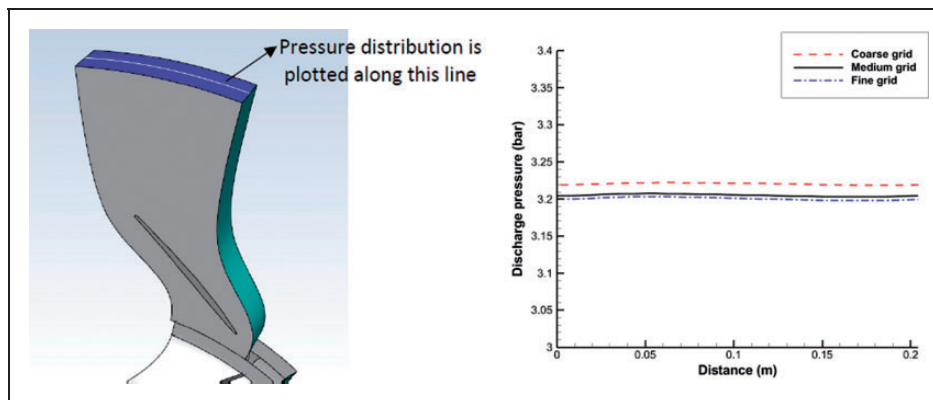


Figure 5. Numerical results for the pressure distribution on a line at the center of the diffuser outlet, obtained with different grid resolutions.

The effects of the number of inlet guide vanes, N_{IGV} , on the performance curve of the compressor are presented in Figure 7. The simulations are performed for $N_{IGV}=7, 11$ and 15 at two IGV inclination angles, $\lambda_{IGV} = -30^\circ$ and $+45^\circ$. As the figure shows, at both IGV inclination angles, the maximum pressure rise has occurred for $N_{IGV}=11$ and the minimum pressure rise has occurred for $N_{IGV}=7$. It can be concluded from Figures 6 and 7 that the effect of N_{IGV} on the surge flow rate is negligible, however, the IGV turning angle has considerable effects on the surge mass flow rate. Compared to the compressor without any IGV, the surge mass flow rate is 8.5% larger at $\lambda_{IGV} = -30^\circ$ while it is 25% lower at $\lambda_{IGV} = +45^\circ$.

The reasons for choosing $N_{IGV} = 7$ and 15 for the numerical simulations are two folds:

- As the numerical results shows (Figure 7), the compressor performance curve is not very sensitive to the number of inlet guide vanes. Therefore, small

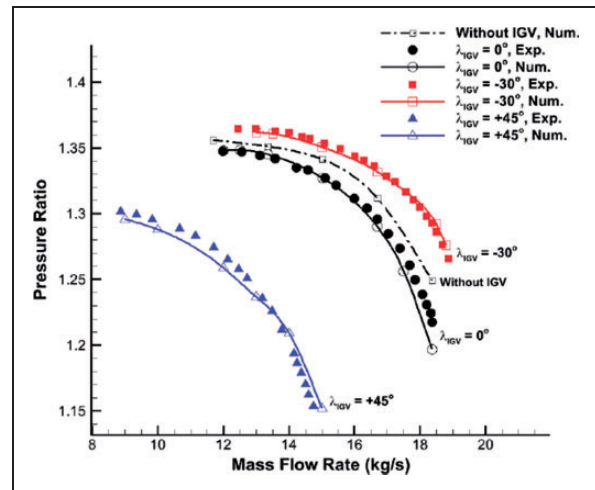


Figure 6. Comparison between numerical results and experimental data presented in the manufacturer's data sheet.

changes in N_{IGV} have no considerable effects on the performance curves of the compressor.

- From the practical point of view, very small or very large values for N_{IGV} is irrelevant due to the geometrical constraints, as shown in Figure 8.

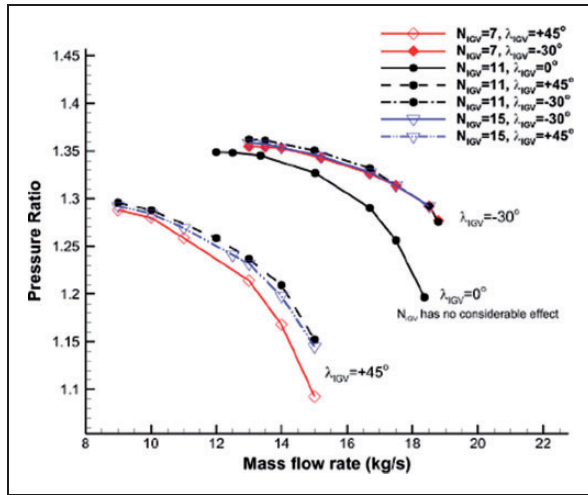


Figure 7. Compressor performance curves at various IGV angles and number of inlet vanes.

The figure also shows that the effects of N_{IGV} on the compressor pressure rise gains weight as the λ_{IGV} increases, in a manner that its effect is negligible at $\lambda_{IGV}=0^\circ$, while it has considerable effects at $\lambda_{IGV}=+45^\circ$. In fact, N_{IGV} has counteracting effects on the impeller aerodynamic performance:

- Increasing N_{IGV} , imposes a higher pressure drop in the inlet passage of the compressor.
- As N_{IGV} increases, the flow angle at the suction surface of the impeller might have a better agreement with that of the λ_{IGV} .
- A higher blockage ratio exists as N_{IGV} increases, especially at lower spans because the vanes are closer to each other near the hub. This will guide the air towards higher span values where the blockage is considerably lower.
- The inlet distortions at larger inclination angles of the IGVs can affect the performance of the impeller. It alters the impeller outlet pressure and velocity distribution.

Therefore, due to these counteracting effects, it is expected that there is an optimum value for N_{IGV} . Figure 9 shows the static pressure distributions on a

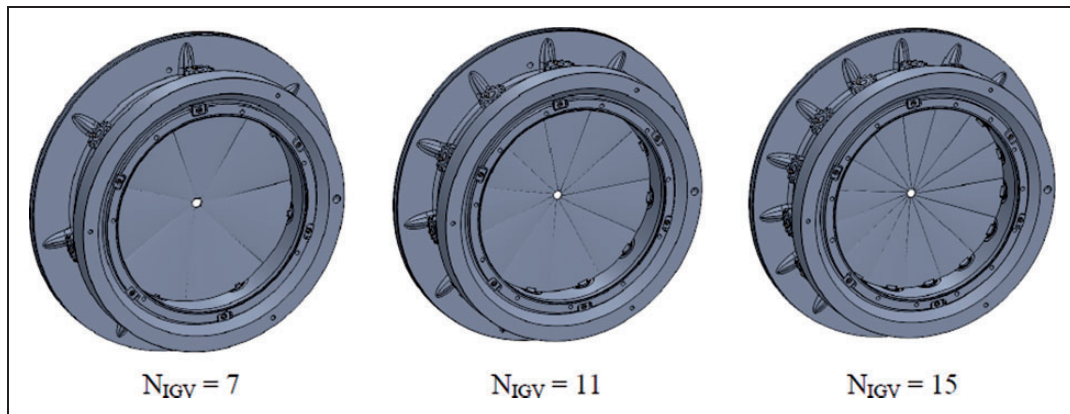


Figure 8. A schematic of the IGV with various number of vanes.

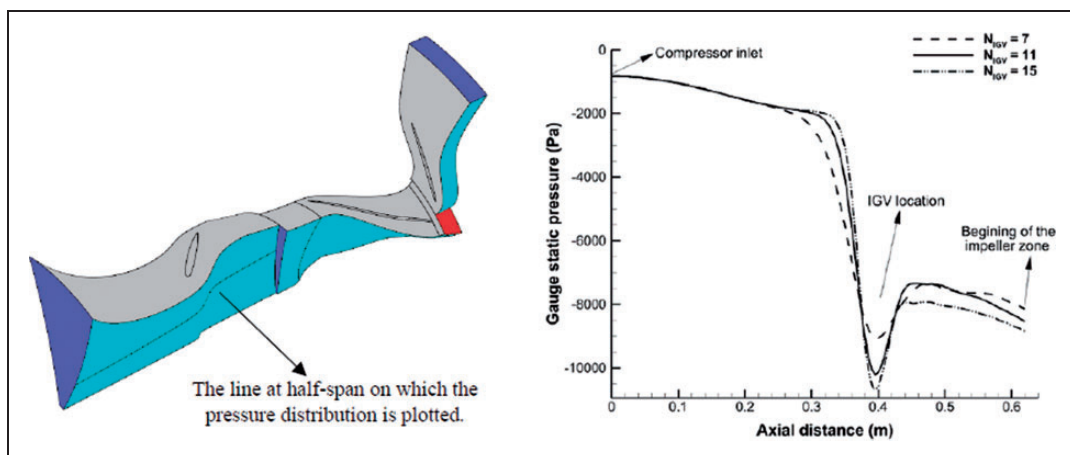


Figure 9. N_{IGV} effects on the pressure distribution on a line on the periodic boundary of the IGV zone at half span and $\lambda_{IGV} = +45^\circ$.

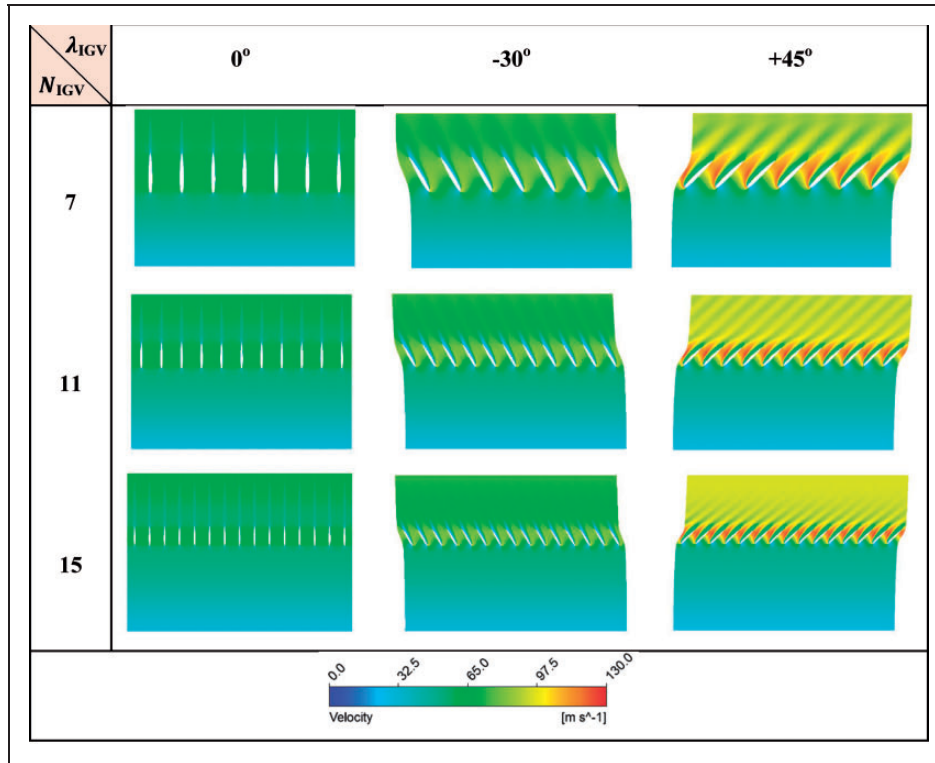


Figure 10. Velocity distributions around the IGV on a mid-span plane in the blade-to-blade view for different number of inlet guide vanes at mass flow rate of 14 kg/s for $\lambda_{IGV} = 0^\circ, -30^\circ$ and $+45^\circ$.

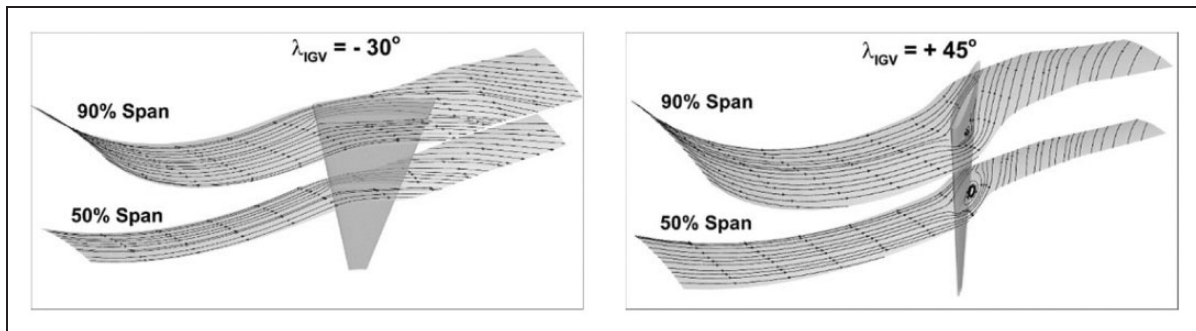


Figure 11. Streamline distributions on two faces located at 50% and 90% span of the IGV zone at mass flow rate of 14 kg/s for two IGV turning angles.

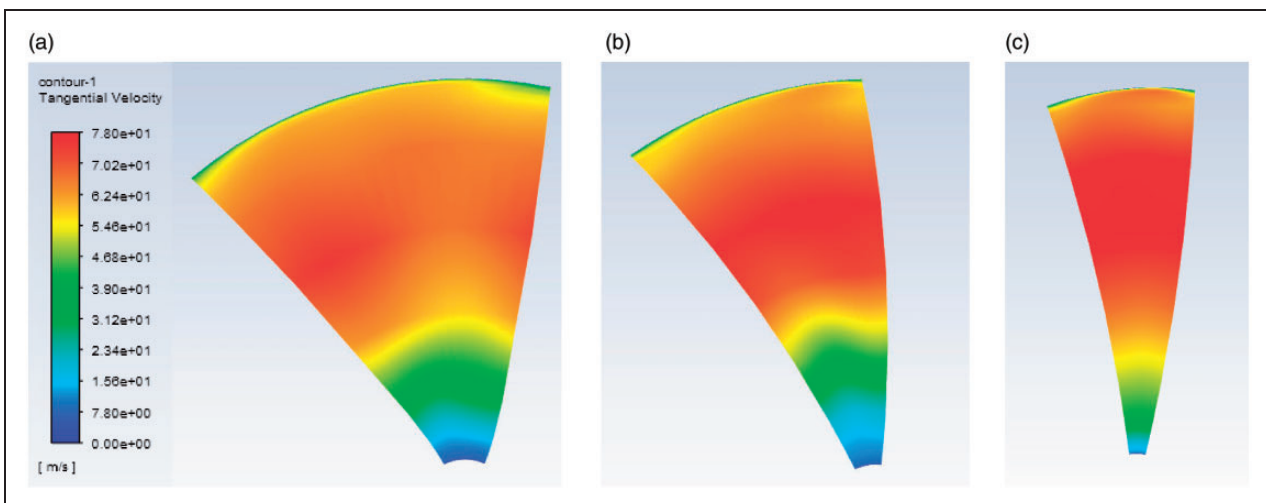


Figure 12. Tangential velocity distributions on the outlet surface of the IGV zone (the green mixing plane shown in Figure 3, at $\lambda_{IGV} = +45^\circ$ and mass flow rate of 14 kg/s.

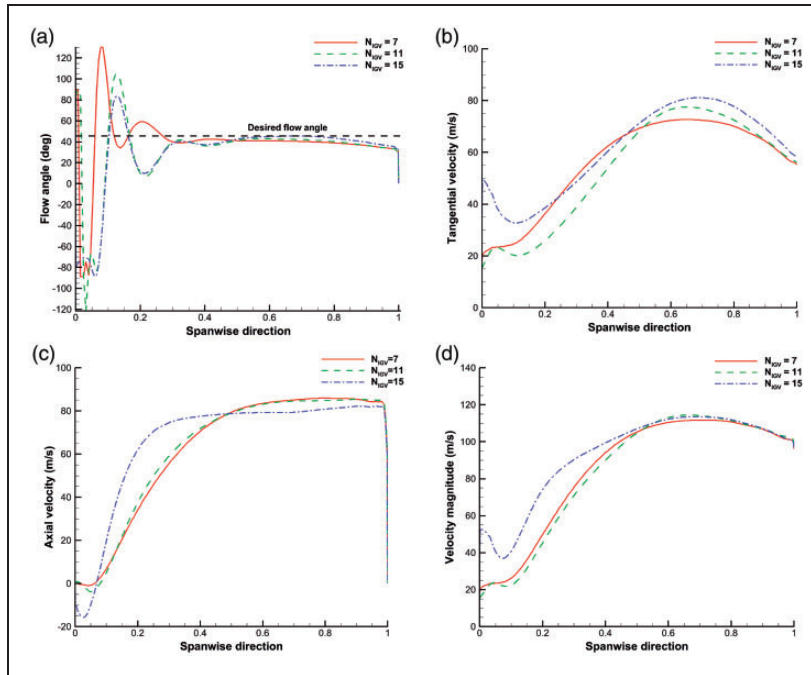


Figure 13. Hub-to-shroud variations of the (a) flow angle (b) circumferential velocity component (c) axial velocity component and (d) velocity magnitude on a line at half pitch, located on the interface between the IGV and impeller zones at $\lambda_{IGV} = +45^\circ$ and mass flow rate of 14 kg/s.

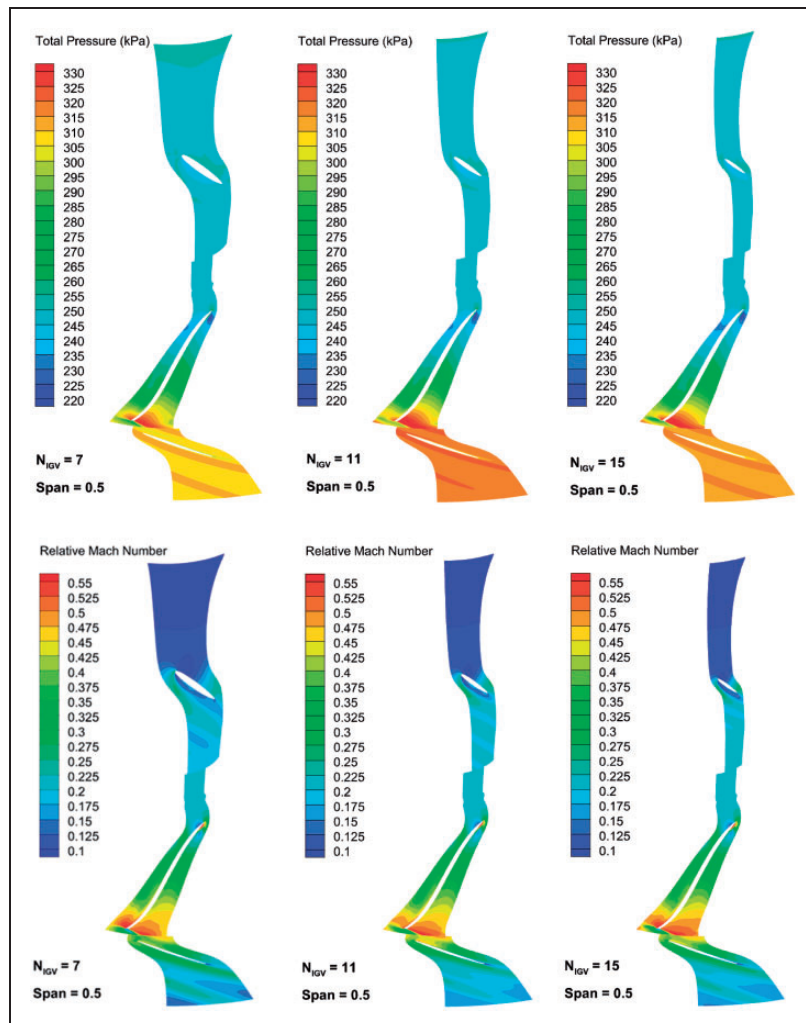


Figure 14. Total pressure and relative Mach number distributions on a plane located at mid-span for $\lambda_{IGV} = +45^\circ$ and mass flow rate of 14 kg/s.

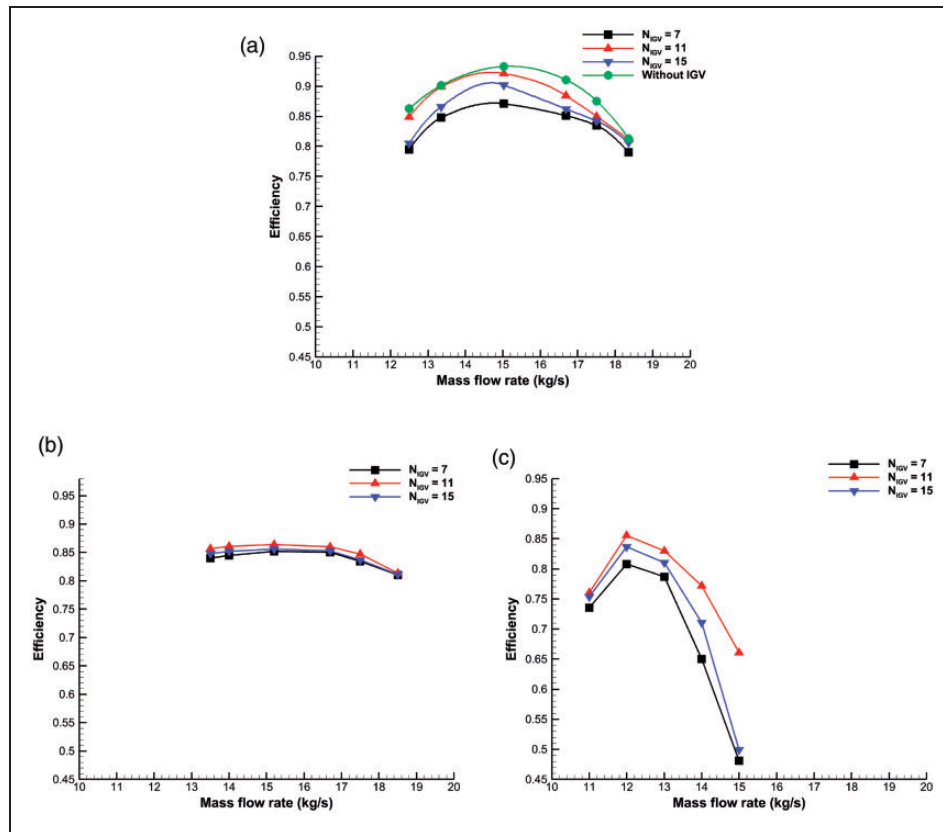


Figure 15. The effects of number of inlet vanes, N_{IGV} , on the compressor efficiency at three IGV angles and without IGV.

line at half span on the periodic boundary of the IGV zone for $\lambda_{IGV} = +45^\circ$ and three different N_{IGV} at mass flow rate of 14 kg/s. As can be seen in the figure, the minimum static pressure occurs at the location of the IGV, where the blockage effect of the vanes causes the flow velocity to increase locally and as a result, the static pressure decreases. Clearly, as the number of inlet guide vanes increases, a more intense pressure drop occurs. It must be noted that the intensity of the local pressure drop is larger at lower spans, due to higher blockage.

The corresponding velocity distributions on a blade-to-blade view at the mid-span position is depicted in Figure 10 for three different N_{IGV} at $\lambda_{IGV} = 0^\circ, -30^\circ$ and $+45^\circ$. As can be seen in the figure, at a constant mass flow rate, as the IGV turning angle increases, the maximum velocity magnitude increase. Furthermore, IGV stall occurs only at $\lambda_{IGV} = +45^\circ$. Figure 10 also shows that as N_{IGV} increases, there is a more uniform velocity distribution at the exit surface of the IGV zone.

Generally, the loss zones in IGV don't propagate into the impeller due to the distance between the inlet vanes and the impeller. To better illustrate the separation zone on the IGV, the streamline distributions on two faces, located at 50% and 90% span of the IGV zone, are depicted in Figure 11. As can be seen in the figure, there is a separation zone on the suction surface of the IGV at $\lambda_{IGV} = +45^\circ$. However, the

effects of this separation zone decays rapidly and it does not reach the impeller.

The distributions of the tangential velocity component at the exit surface of the IGV zone are shown in Figure 12 for the three studied N_{IGV} . The area of this surface decreases as N_{IGV} increases, due to the requirements of the periodic boundary conditions. The non-uniformity in the tangential velocity component can be clearly seen in this figure for $N_{IGV} = 7$, while there is almost a uniform tangential velocity distribution in the pitch-wise direction for $N_{IGV} = 15$.

The hub-to-shroud variations of the velocity components on a line at half pitch, located on the interface between the IGV and impeller zones are presented in Figure 13. In this figure, the variations of the velocity magnitude, axial velocity, tangential velocity and the flow angle are plotted on the specified line. As can be seen in the Figure 13(a), the flow angle is almost equal to λ_{IGV} at span > 0.5 . At span < 0.2 , a relatively small negative axial velocity component can also be seen which can block the flow. The flow angle deviation near the hub occurs only at large turning angles ($\lambda_{IGV} = +45^\circ$) when the flow is reaching the nose of the impeller cap. A small vortex-like structure forms at this region, which doesn't exist at lower values of the IGV turning angle. In this region, the flow has to climb up from near the zero radial coordinate up to the impeller cap. Furthermore, as can be seen in Figure 1(a), the inlet

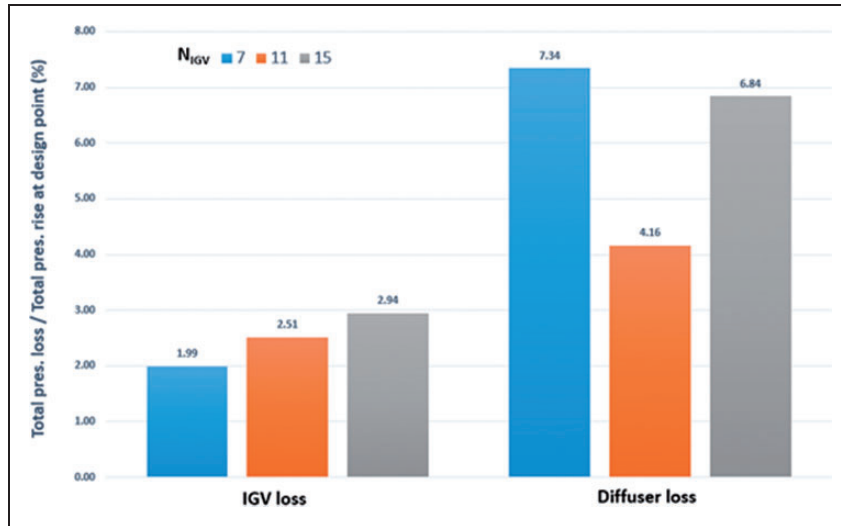


Figure 16. Total pressure losses in the IGV and diffuser zones for different number of N_{IGV}

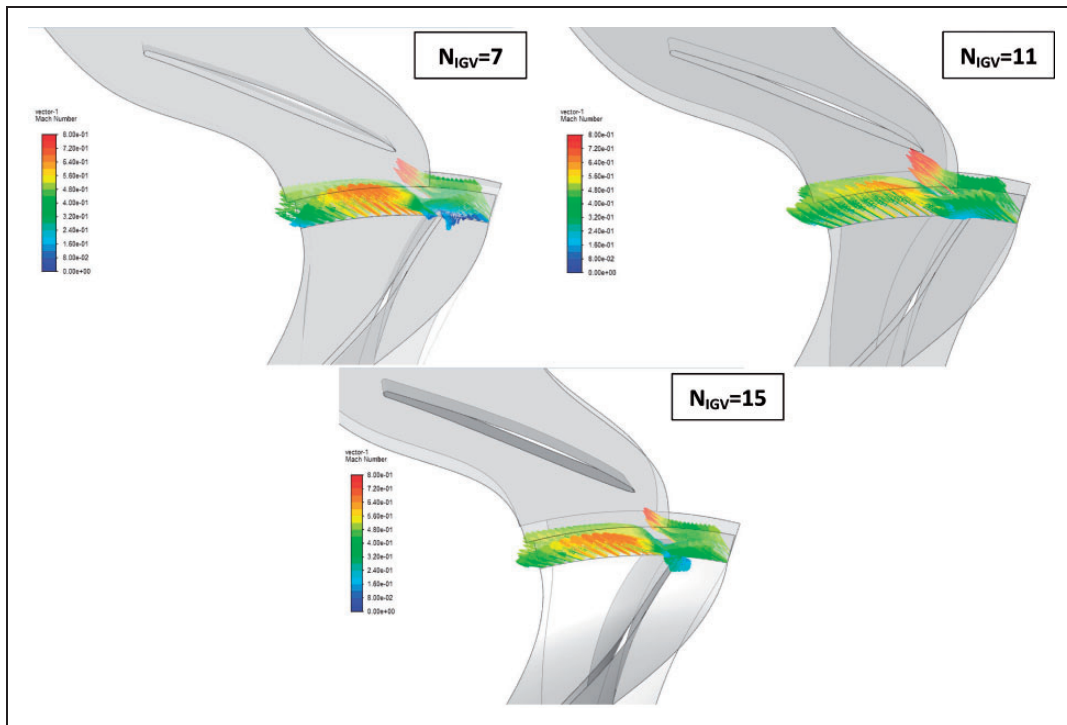


Figure 17. Velocity vectors distributions, colored by Mach number, on the interface between the impeller zone and diffuser zone at $\lambda_{IGV} = +45^\circ$ and mass flow rate of 14 kg/s.

passage diameter is decreasing towards the impeller. In other words, the impeller diameter is smaller than the diameter of the section where these velocity profiles are plotted. The strength of the negative axial velocity grows as N_{IGV} increases. Figure 13(d) shows that the average velocity magnitude is larger at $N_{IGV}=15$ due to larger blockage, while the flow angle is closer to λ_{IGV} .

The contours of the total pressure and Mach number distributions on a plane located at mid-span for $\lambda_{IGV} = +45^\circ$ and mass flow rate of 14 kg/s are shown in Figure 14 for different values of N_{IGV} .

As the figure shows, the Mach number after the IGV increases as the N_{IGV} increases. However, the total pressure is larger at the diffuser zone for $N_{IGV}=11$. To determine the optimum number of inlet guide vanes, the variations of the torque-based total-to-total efficiency as a function of the mass flow rate at $\lambda_{IGV} = 0^\circ, -30^\circ$ and $+45^\circ$ are presented in Figure 15 for different N_{IGV} . At all of the IGV angles, the maximum efficiency has occurred at $N_{IGV} = 11$ and the minimum efficiency at $N_{IGV} = 7$.

In order to find the sources of the losses, the total pressure losses occurred in the IGV and diffuser zones

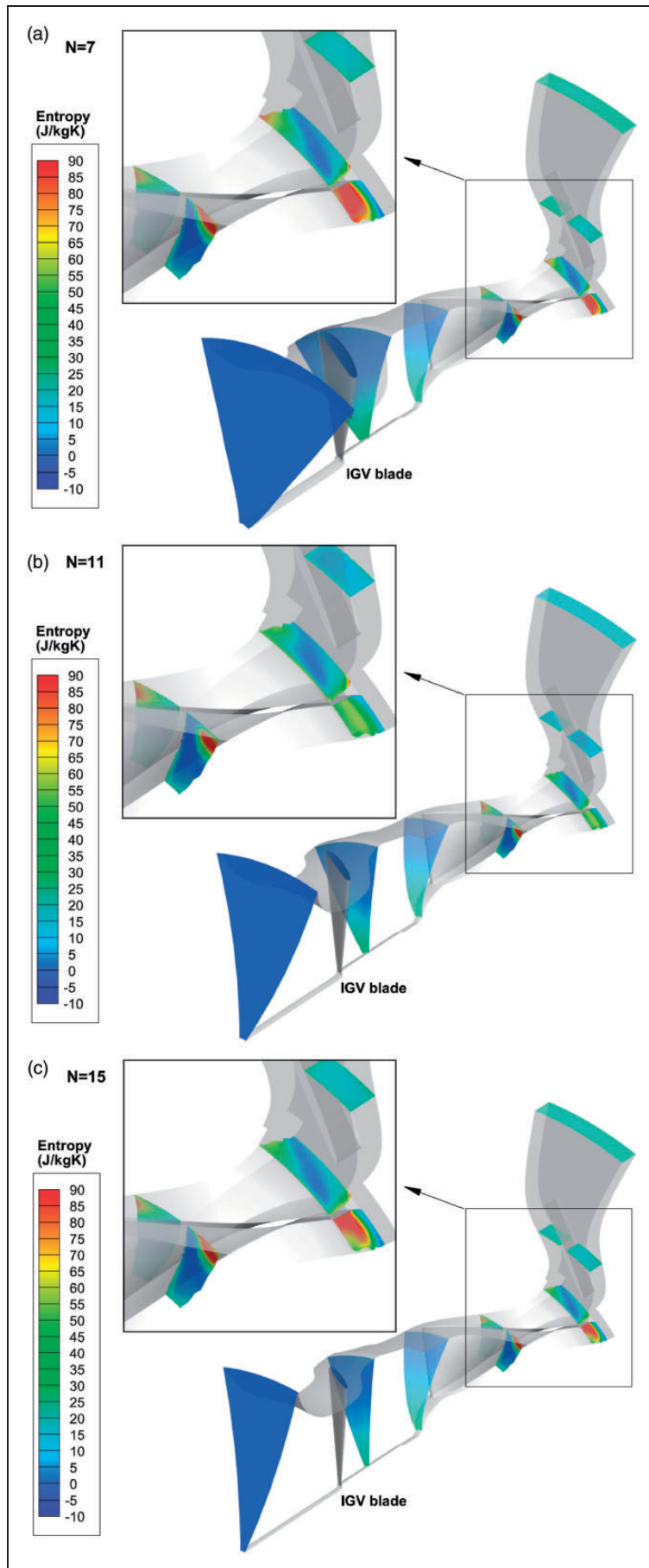


Figure 18. Entropy distributions on several meridional locations from the compressor inlet up to the outlet for various N_{IGV} at $\lambda_{IGV} = +45^\circ$ and mass flow rate of 14 kg/s.

at various N_{IGV} are presented in Figure 16 for $\lambda_{IGV} = +45^\circ$ and mass flow rate of 14 kg/s. As the figure shows, the IGV zone losses increases as N_{IGV} increases. However, the diffuser losses are minimum at $N_{IGV} = 11$. The losses occurred in the diffuser zone depends on the exit velocity distribution of the impeller entering the diffuser.

Figure 17 illustrates the velocity vectors on the interface between the impeller and diffuser zones. The jet-wake structure can be well observed in this figure, where the wake zone is minimum at $N_{IGV} = 11$. This might be the reason for lower losses at this N_{IGV} . The contours of entropy on several meridional locations from the compressor inlet up to the outlet for various N_{IGV} at $\lambda_{IGV} = +45^\circ$ and mass flow rate of 14 kg/s are presented in Figure 18. As can be seen in the figure, the entropy generated in the impeller is more intense near the shroud. It is also more concentrated at the suction surface of the impeller, where there is the wake flow.

Conclusions

Due to the widespread applications of variable inlet guide vanes (VIGVs) for efficient throttling and altering the operating range of the centrifugal compressors, in the current study the effects of the number of inlet vanes on the performance of an industrial compressor are investigated. The three-dimensional numerical simulations are performed based on the single passage model using the Ansys-Fluent commercial software. The study is performed on a single-stage high-flow rate compressor, originally designed and fabricated by Siemens. The simulations are carried out for three different number of guide vanes and three IGV inclination angles of 0, -30 and $+45$ degrees. The main findings of the current study can be summarized as follows:

- Comparing the obtained numerical results for the pressure-rise vs flow-rate curves at different angles of the IGVs with those of the compressor data-sheet confirmed the high accuracy of the numerical results.
- At the fully-open condition, the number of inlet vanes doesn't have considerable effects on the performance curve of the compressor. Therefore, if the compressor is intended to seldomly operate at the off-design conditions using the VIGVs, there is lower sensitivity on the number of inlet guide vanes.
- As the IGV inclination angle increases, the number of inlet vanes plays a considerable role in the compressor efficiency and performance curve. Nevertheless, the effects are more profound on the efficiency curves in comparison to the pressure-rise curves.
- Increasing the number of inlet guide vanes, imposes a higher pressure drop in the inlet passage

of the compressor, while generating a more uniform velocity distribution at the suction surface of the impeller. However, the inlet distortions can deteriorate the aerodynamic performance of the impeller.

- An optimum number of inlet guide vanes can be found for a centrifugal compressor to reach higher efficiencies at large inclination angles of the inlet guide vanes.

For the future research, it is intended to study the unsteady effects of adding IGV with various number of vanes on the aerodynamic performance of the full-model of the centrifugal compressor.

Acknowledgement

The authors would like to express their gratitude to the PSP company, *Mr. Hossein Khatibi* and *Mr. Reza Ghavidel* for providing funds for this project.

Declaration of Conflicting Interests

The author(s) declared no potential conflicts of interest with respect to the research, authorship, and/or publication of this article.

Funding

The author(s) received no financial support for the research, authorship, and/or publication of this article.

ORCID iD

M Anbarsooz  <https://orcid.org/0000-0002-8133-5552>

References

1. Boyce MP. *Centrifugal compressors: a basic guide*. Tulsa, OK: PennWell, 2003.
2. Rodgers C. Impeller stalling as influenced by diffusion limitations. *J Fluids Eng Trans ASME* 1977; 99: 84–93.
3. Harada H. Performance characteristics of shrouded and unshrouded impellers of a centrifugal compressor. *J Eng Gas Turbines Power* 1985; 107: 528–533.
4. Zhao H, Wang Z, Yu H, et al. Numerical investigation of shock effects on performance and flow field in a transonic centrifugal impeller. In: *Proc. ASME turbo expo*, Seoul, 13–17 June 2016.
5. Senoo Y and Nakase Y. An analysis of flow through a mixed flow impeller. *J Eng Gas Turbines Power* 1972; 94: 43–50.
6. Ito S, Okada S, Kawakami Y, et al. Suppression of secondary flows in a transonic centrifugal compressor impeller using an inverse design method based on meridional viscous flow analysis. In: *AJKFluids ASME - JSME - KSME joint fluids engineering conference*, San Francisco, CA, 28 July–1 August 2019.
7. Kim S, Park J and Baek J. A numerical study of the effects of blade angle distribution on the performance and loss generation of centrifugal compressor impellers. *Proc IMechE, Part A: J Power and Energy* 2012; 226: 208–217.
8. Shibata T, Yagi M, Nishida H, et al. Performance improvement of a centrifugal compressor stage by

- increasing degree of reaction and optimizing blade loading of a 3D impeller. *J Turbomach* 2011; 133: 021004 (8 pages).
9. Zangeneh M, Goto A and Harada H. On the design criteria for suppression of secondary flows in centrifugal and mixed flow impellers. *J. Turbomach* 1998; 120: 723–735.
 10. Xie X, Li Z, Zhu B, et al. Suppression of secondary flows in a centrifugal impeller by optimisation design. *EC* 2020; 37: 3023–3044.
 11. Miyamoto H, Nakashima Y and Ohba H. Effects of splitter blades on the flows and characteristics in centrifugal impellers. *JSME Int Journal, Ser. 2 Fluids Eng. Heat Transf Power, Combust. Thermophys Prop* 1992; 35: 238–246.
 12. Anish S and Sitaram N. Computational investigation of impeller-diffuser interaction in a centrifugal compressor with different types of diffusers. *Proc IMechE, Part A: J Power and Energy* 2009; 223: 167–178.
 13. Krain H. A study on centrifugal impeller and diffuser flow. *J Eng Gas Turbines Power* 1981; 103: 688–697.
 14. Engeda A. The unsteady performance of a centrifugal compressor with different diffusers. *Proc IMechE, Part A: J Power and Energy* 2001; 215: 585–599.
 15. El-Zahaby AM, Kabeel AE, Elsayed SS, et al. CFD analysis of flow fields for shrouded wind turbine's diffuser model with different flange angles. *Alexandria Eng J* 2017; 56: 171–179.
 16. Marconcini M, Rubecchini F, Arnone A, et al. Numerical analysis of the vaned diffuser of a transonic centrifugal compressor. *J Turbomach* 2010; 132: 1–8.
 17. Hildebrandt A and Genrup M. Numerical investigation of the effect of different back sweep angle and exducer width on the impeller outlet flow pattern of a centrifugal compressor with vaneless diffuser. *J Turbomach* 2007; 129: 421–433.
 18. Ziegler KU, Gallus HE and Niehuis R. A study on impeller-diffuser interaction – part II: detailed flow analysis. *J Turbomach* 2003; 125: 183–192.
 19. Rodgers C. Centrifugal compressor inlet guide vanes for increased surge margin. *J Turbomach* 1991; 113: 696–702..
 20. Ishino M, Iwakiri Y, Bessho A, et al. Effects of variable inlet guide vanes on small centrifugal compressor performance. In: *Proc. ASME turbo expo*, Indianapolis, IN, 7–10 June 1999.
 21. Mohtar H, Chesse P, Chalet D, et al. Effect of casing treatment and variable axial guide vanes on a turbocharger compressor performance. In: *Proc. ASME turbo expo*. Orlando, Florida, USA, 2009, pp.47–54.
 22. Mohtar H, Chesse P, Yammine A, et al. Variable inlet guide vanes in a turbocharger centrifugal compressor: Local and global study. SAE Technical Paper, 2008.
 23. Toussaint M and Podevin P. Guide-Vanes upstream the impeller of centrifugal compressor. *5th Eur Conf Turbomach Fluid Dyn Thermodyn* 2003: 67–74.
 24. Xiao J, Gu C, Shu X, et al. Performance analysis of a centrifugal compressor with variable inlet guide vanes. *Front Energy Power Eng China* 2007; 1: 473–476.
 25. Zemp A, Kammerer A and Abhari RS. Unsteady computational fluid dynamics investigation on inlet distortion in a centrifugal compressor. *J. Turbomach* 2010; 132: 031015 (9 pages).
 26. Tan J, Wang X, Qi D, et al. The effects of radial inlet with splitters on the performance of variable inlet guide vanes in a centrifugal compressor stage. *Proc IMechE, Part C: J Mechanical Engineering Science* 2011; 225: 2089–2105.
 27. Benini E and Tourlidakis A. Design optimization of vaned diffusers for centrifugal compressors using genetic algorithms. In: *15th AIAA computational fluid dynamics conference*, Anaheim, CA, 11–14 June 2001.
 28. Halawa T, Alqaradawi M, Gadala MS, et al. Numerical investigation of rotating stall in centrifugal compressor with vaned and vaneless diffuser. *J Therm Sci* 2015; 24: 323–333.
 29. Anbarsooz M, Mazloum M and Moghadam DG. Converging–diverging ducts for efficient utilization of low-grade wind energy: numerical and experimental studies. *J Renew Sustain Energy* 2020; 12: 023304.
 30. Anbarsooz M. A numerical study on wind dams: a novel approach to enhance wind potential using natural barriers. *Energy Convers Manag* 2020; 205: 112454.
 31. Jiao K, Sun H, Li X, et al. Numerical simulation of air flow through turbocharger compressors with dual volute design. *Appl Energy* 2009; 86: 2494–2506.
 32. ANSYS, Inc. ANSYS manual, Release 19.0., n.d.
 33. Anbarsooz M. Aerodynamic performance of helical Savonius wind rotors with 30° and 45° twist angles: experimental and numerical studies. *Proc IMechE, Part A: J Power and Energy* 2016; 230: 523–534.
 34. Amiri M and Anbarsooz M. Improving the energy conversion efficiency of a Savonius rotor using automatic valves. *J. Sol Energy Eng Trans ASME* 2019; 141: 31010–31017.
 35. Kianifar A and Anbarsooz M. Blade curve influences on the performance of savonius rotors: experimental and numerical. *Proc IMechE, Part A: J Power and Energy* 2011; 225: 343–350.
 36. Cornelius C, Biesinger T, Galpin P, et al. Experimental and computational analysis of a multistage axial compressor including stall prediction by steady and transient CFD methods. *J. Turbomach* 2014; 136, DOI: <https://doi.org/10.1115/1.4025583>.
 37. Stewart M. Dynamic compressors. In: Stewart MBT-SPO (ed.) *Surface production operations*. Boston: Gulf Professional Publishing, 2019, pp.527–653.
 38. Engeda A. Experimental and numerical investigation of the performance of a 240 kW centrifugal compressor with different diffusers. *Exp Therm Fluid Sci* 2003; 28: 55–72.
 39. Goldberg U, Peroomian O and Chakravarthy S. A wall-distance-free K- ϵ model with enhanced near-wall treatment. *J Fluids Eng Trans ASME* 1998; 120: 457–462.
 40. Versteeg HK and Malalasekera W. Y plus. In: *Introduction to Computational Fluid Dynamics*. Hong Kong. Pearson; 2nd edition, 2007, p.72.
 41. Najjar YSH and Akeel SAMS. Effect of prewhirl on the performance of centrifugal compressors. *Int J Rotating Mach* 2002; 8: 397–401.
 42. Benini E. Optimal Navier-Stokes design of compressor impellers using evolutionary computation. *Int J Comut Fluid Dyn* 2003; 17: 357–369.